JBIC Journal of Biological Inorganic Chemistry (2021) 26:135–147
https://doi.org/10.1007/s00775-020-01843-7

ORIGINAL PAPER

Phototriggered cytotoxic properties of tricarbonyl manganese(I) complexes bearing α-diimine ligands towards HepG2

Ahmed M. Mansour[1] · Krzysztof Radacki[2] · Rabaa M. Khaled[1] · Marwa H. Soliman[1] · Nour T. Abdel-Ghani[1]

Received: 21 October 2020 / Accepted: 1 December 2020 / Published online: 27 February 2021

Abstract

Reaction between bromo tricarbonyl manganese(I) and *N,N′*-bis(phenyl)-1,4-diaza-1,3-butadiene ligands, bearing different electron-donating and electron-withdrawing groups R = OCH_3, Cl, and NO_2 in the *ortho*- and *para*-positions on the phenyl substituent, afforded [$MnBr(CO)_3$(N–N)] complexes. The influence of the character and position of the substituent on the dark stability and carbon monoxide releasing kinetics was systematically investigated and correlated with the data of the time-dependent density functional theory calculations. The combined UV/Vis and IR data clearly revealed that the aerated solutions of [$MnBr(CO)_3$(N–N)] in either coordinating or noncoordinating solvents are dark stable and the fluctuations observed during the incubation period especially in the case of the nitro derivatives may be attributed to the exchange of the axial bromo ligand with the coordinating solvent molecules. The free ligands and nitro complexes were non-cytotoxic to HepG2 cells under both the dark and illumination conditions. In the dark, Mn(I) compounds, incorporating *o*-OCH_3 and *o*-Cl, exhibited excellent cytotoxicity with IC_{50} values of 18.1 and 11.8 μM, while their *para*-substituted analogues were inactive in the dark and active upon the irradiation at 365 nm with IC_{50} values of 5.7 and 6.7 μM, respectively.

Keywords Photoactivatable · α-Diimines · Mn(i) compounds · HepG2 · Carbon monoxide

Introduction

It is well known that the toxicity of carbon monoxide ''the silent killer gas'' is attributed to the strong affinity to haemoglobin compared to oxygen. Small quantities of CO are enzymatically produced by the action of heme oxygenase (HO) enzymes on heme [1]. To date, CO displays remarkable useful biological effects including the reduction of the chemotherapeutic resistance and proliferation of cancer cells [2]. For example, CO enhanced the response of the cancerous breast cells to doxorubicin-mediated death by about 40%. Promotion of wound healing, participation in essential signaling processes and the cyto-protection during the inflammations are some of the other beneficial biological effects of CO in the concentration range of 10–250 ppm [3]. CO has a role in the regulation of vascular tonus in conduit arteries [4]. Due to the non-selectivity of CO to metal-based biomolecules, it is not recommended to administrate CO by inhalation. Carbon monoxide releasing molecules (CORMs) were lately launched for administration of well-controlled quantities of CO to tissues upon the activation with either internal or external sources. The fact that CO reacts primarily with low oxidation states transition metal ions encouraged the research groups to investigate some metal carbonyls as prodrugs for carbon monoxide. The first transition metal-based CORMs, [$Mn_2(CO)_{10}$] (CORM-1) and [$RuCl(\mu\text{-}Cl)(CO)_3]_2$ (CORM-2), were introduced by Motterlini's research group [5]. Because of the poor water solubility of the first generation CORMs, more biocompatible Ru(II)-based complex incorporating amino acid, [RuCl(glycinato)$(CO)_3$] (CORM-3) was introduced. CORM-3 is stable in the aqueous acidic media, but liberates CO in physiological buffers and human plasma. CORM-3 has a cardioprotective effect as well as the ability to prolong the survival of the transplanted hearts in mice [6]. Motterlini's complexes were the milestone for researchers to investigate the ability of using metal

✉ Ahmed M. Mansour
mansour@sci.cu.edu.eg; inorganic_am@yahoo.com

[1] Department of Chemistry, Faculty of Science, Cairo University, Gamma Street, Giza 12613, Cairo, Egypt

[2] Institut Für Anorganische Chemie, Julius-Maximilians-Universität Würzburg, Am Hubland, 97074 Würzburg, Germany

carbonyl complexes as prodrugs for CO delivery and that encouraged to continue with the trials to make CO clinical applications possible, using CORMs based on other metal ions and co-ligands. As reported, the release of CO from CORMs can be achieved as follows: use of light [5], change of pH [7], unusual physiological conditions [8], thermally [1], enzymatically [9–11], increase in ROS concentration [12], ligand exchange [1], and by the change the metal oxidation state [13, 14]. The use of light as a triggering method to release CO from metal carbonyls has permitted facile control of location, dosage of CO, and initiative time [15].

Tricarbonyl manganese(I) complexes received significant interest because of their promising photophysical and biological applications [16–25]. Initially, the ability of $[Mn(CO)_3(tpm)]PF_6$ (tpm = tris(pyrazolyl)methane) to release CO and the resulting photoinduced cytotoxicity properties upon the illumination at 365 nm were reported [26]. The CO release properties of $[MnBr(CO)_3(pbt)]$ (pbt = 2-(2-pyridyl)benzothiazole)), which promotes CO-triggered death of human breast cancer cells upon the illumination with visible light, were studied [24]. *Fac*-$[MnBr(CO)_3L^{2,6-prop}]$ ($L^{2,6-prop}$: *N,N′*-bis(2,6-diisopropylphenyl)-1,4-diaza-1,3-butadiene) displayed facile photoinduced CO release upon the exposure to visible light (550 nm) [27]. Recently, two *fac*-$[MnBr(CO)_3(N–N)]$ series, incorporating *N,N*-bidentate Schiff base ligands, capable of releasing CO at 525 nm, showed a good photo cytotoxic activity against HepG2 attributing to the nature of the iCORM (the residue after CO release) [28].

Owing to the promising antimicrobial [16, 29, 30] and cytotoxicity [22, 24, 26] of PhotoCORMs (the name introduced by Ford specifying the category of the photoinduced CORMs) [15] functionalized with *N,N*-bidentate ligands, we designed a series of photo induced tricarbonyl Mn(I) compounds (**7–12**) (Scheme 1) derived from Schiff-base ligands, bearing different electron-donating and electron-withdrawing groups (R=OCH_3, Cl, and NO_2) (**1–6**). These derivatives were chosen to investigate the influence of the character and position of the substituent on the phenyl ring on the CO release kinetics of the investigated compounds. The dark stability and the ability of **7–12** to act as prodrugs for CO were studied by UV/Vis and IR spectroscopy. The cytotoxicity of **1–12** towards HepG2 was evaluated both in the dark and upon the illumination.

Results and discussion

Synthesis and characterization

Six functionalized Schiff-base ligands (**1–6**) (Scheme 1) were synthesized by condensation of ethylenediamine

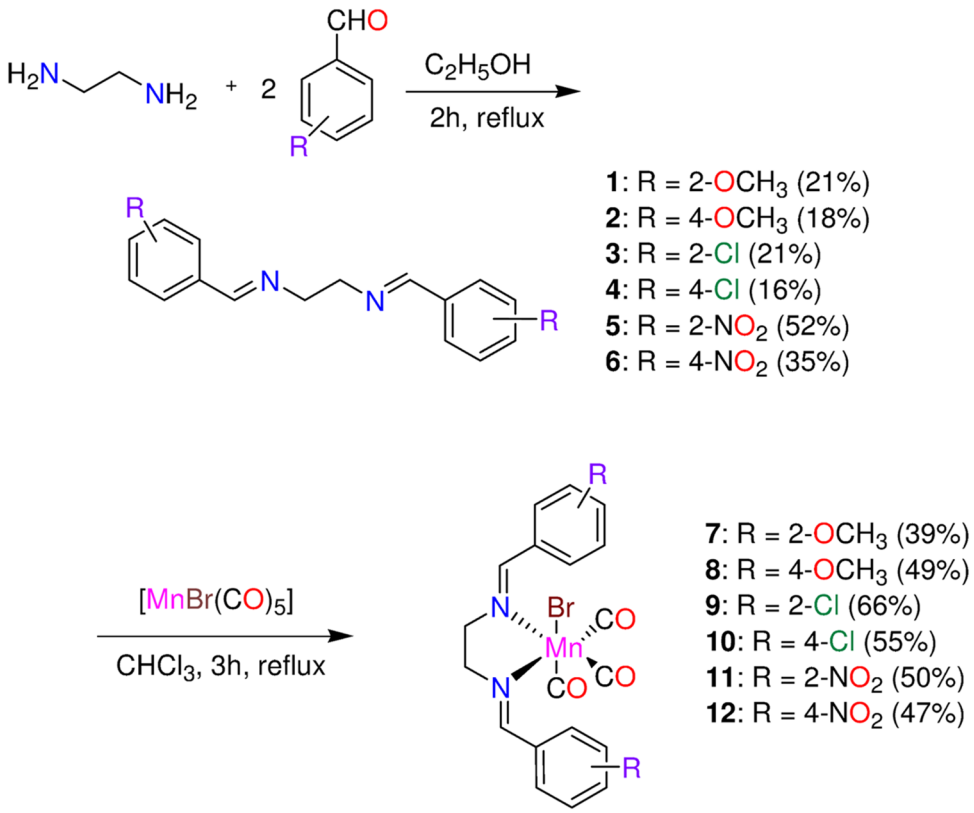

Scheme 1 Synthesis of Schiff-base ligands (**1–6**) and their photoactivatable bromo tricarbonyl Mn(I) complexes (**7–12**)

with two equivalents of *ortho*- and *para*-substituted benzaldehydes (R = OCH_3, Cl, and NO_2). The six ligands were obtained in a pure form. The structures of the ligands were elucidated by IR (Fig. S1), NMR (^1H and $^{13}C\{^1H\}$) (Figs. S2 and S3) and elemental analysis. The ^1H NMR signal of –CH=N– group of **1**–**6** is observed in the range of 8.24–8.64 ppm. A systematic downfield shift of the ^1H NMR signal of –CH=N– group by changing the character of the substituent in the *para*-position of the benzaldehyde residue from the electron-donating (8.24 ppm, R = OCH_3) to the electron-withdrawing character (8.33 ppm, R = Cl; 8.51, R = NO_2) is observed. Changing the position of the substituent from *para* to *ortho* caused a noticeable downfield shift for the same signal. Reaction of **1**–**6** with [$MnBr(CO)_5$] in chloroform, with exclusion of light, gave *facial* bromo tricarbonyl Mn(I) complexes **7**–**12**, which were characterized by IR (Fig. S4), NMR (^1H (Fig. S5) and $^{13}C\{^1H\}$ (Fig. S6)), ESI MS, single crystal X-ray diffraction and elemental analysis. The IR spectra of **7**–**10** show two prominent bands at around 2016–2022 and 1905–1908 cm^{-1}, which are assigned to the symmetrical and anti-symmetrical stretching modes of the tricarbonyl Mn(I) moiety. The nitro complexes (**11** and **12**) show three intense ν(C≡O) bands at (2021, 1937, 1902) and (2021, 1945, 1912) cm^{-1}, respectively. The ^1H NMR signal of the –CH=N– group shifts from 8.24–8.64 ppm in **1**–**6** to 8.96–9.45 ppm in **7**–**12** upon the coordination to the metal ion. The broadness of the NMR spectra may be due to quadrupolar nuclear effect and long relaxation time. For **7**, **8**, and **10**, the two –CH=N– groups are non-isoenergetic and thus two ^1H NMR signals are observed at two different chemical shifts (9.13, 9.07), (9.11, 8.96), and (9.23, 9.12) ppm that may be attributed to the intermolecular hydrogen bond as evidenced by X-ray crystallographic analysis (*vide infra*).

Crystal structures

Single crystals of **7**, **8, 10**, and **11**, appropriate for X-ray crystallographic analysis, were grown by diffusion of *n*-hexane into the solutions of the tricarbonyl manganese(I) complexes in CH_2Cl_2. Applicable single-crystal X-ray diffraction parameters are tabulated in Table S1. X-ray crystallographic analysis indicates a distorted octahedral stereochemistry around the Mn(I) ion in the four cases as shown in Fig. 1 and Fig. S7. The bond lengths and angles around the metal ion are given in Fig. 1 and Table S2. In each case, the three CO ligands are coordinated to Mn(I) in a facial mode, two nitrogen atoms of a bidentate Schiff-base ligand and bromo ligand complete the octahedral geometry. The difference between the corresponding bond lengths in **8** and **10** is in the range of 0.001–0.005 Å (3sigma = 0.03) except for Mn–C2, Mn–C3 and Mn–N5_2 bond in which the difference is 0.008–0.012 Å. The root means square difference between the parameters of **8** and **10** is 0.032.

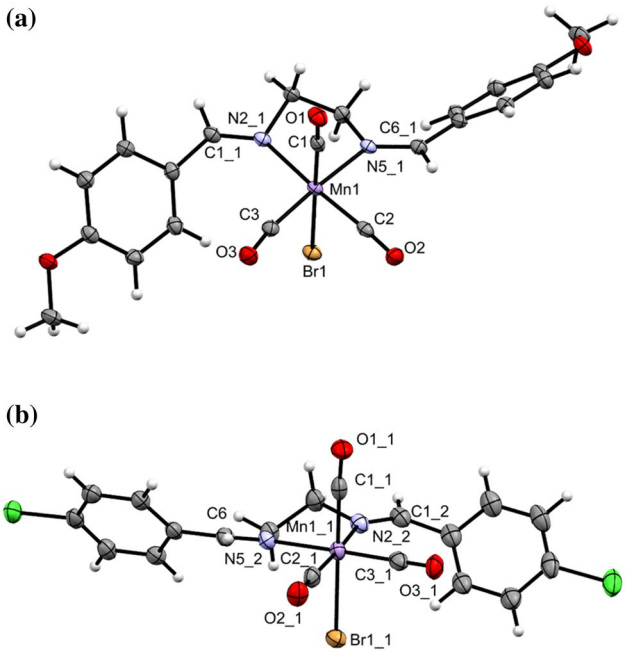

Fig. 1 **a** Molecular structure of complex **8** (thermal ellipsoids are shown at 50% probability level). Mn–C1 1.807(3), Mn–C2 1.805(3), Mn–C3 1.809(2), Mn–N2_1 2.073(3), Mn–N5_1 2.062(2), Mn–Br 2.5367(4), C1–O1 1.139(3), C2–O2 1.140(4), C3–O3 1.152(3), C1–Mn–C2 91.5(1), C1–Mn–C3 87.8(1), C1–Mn–N2_1 90.0(1), C1–Mn–N5_1 94.2(1), C1–Mn–Br 179.07(9), C2–Mn–C3 84.1(1), N2_1–Mn–C2 175.0(1), C2–Mn–N5_1 93.4(1), C2–Mn–Br 87.65(8), N2_1–Mn–C3 100.7(1), C3–Mn–N5_1 176.8(1), C3–Mn–Br 91.75(8), N2_1–Mn–N5_1 81.76(9), N2_1–Mn–Br 90.92(6), and N5_1–Mn–Br 86.25(6); **b** molecular structure of complex **10** (thermal ellipsoids are shown at 50% probability level). Mn–C1_1 1.804(3), Mn–C2_1 1.817(3), Mn–C3_1 1.801(2), Mn–N2_2 2.078(2), Mn–N5_2 2.073(2), Mn–Br1_1 2.5319(5), C1_1–O1 1.137(4), C2_1–O2 1.138(4), C3_1–O3 1.153(3), C1_1–Mn–C2_1 92.5(1), C1_1–Mn–C3_1 88.0(1), C1_1–Mn–N2_2 90.8(1), C1_1–Mn–N5_2 92.4(1), C1_1–Mn–Br1_1 179.67(9), C2_1–Mn–C3_1 85.8(1), N2_2–Mn–C2_1 173.3(1), C2_1–Mn–N5_2 92.3(1), C2_1–Mn–Br1_1 87.22(8), N2_2–Mn–C3_1 100.2(1), C3_1–Mn–N5_2 178.1(1), C3_1–Mn–Br1_1 91.81(9), N2_2–Mn–N5_2 81.61(8), N2_2–Mn–Br1_1 89.57(6) and N5_2–Mn–Br1_1 87.74(6)

The crystal data of **8** and **10** were compared to those of the closely published compound: [$MnBr(CO)_3L^{2,6-prop}$] ($L^{2,6-prop}$: *N,N′*-bis(2,6-diisopropylphenyl)-1,4-diaza-1,3-butadiene) [27]. Exciting, the mean Mn–N bond length in **8** (2.068 Å) and **10** (2.076 Å) is slightly longer than the mean value (2.052 Å) of [$MnBr(CO)_3L^{2,6-prop}$]. Also, the Mn–Br bond lengths in **8** (2.5367(4) Å) and **10** (2.5319(5) Å) are longer than that observed in [$MnBr(CO)_3L^{2,6-prop}$] (2.517 Å). The axial Br–Mn–C1 angles in **8** (179.07(9)°) and **10** (179.67(9)°) approach the linearity that compares well with the published [$MnBr(CO)_3$(α-diamine)] [22, 28], but deviate significantly from that seen in [$MnBr(CO)_3L^{2,6-prop}$] (172.51°). The discrepancy between our crystal data and that observed in [$MnBr(CO)_3L^{2,6-prop}$] may be attributed to the

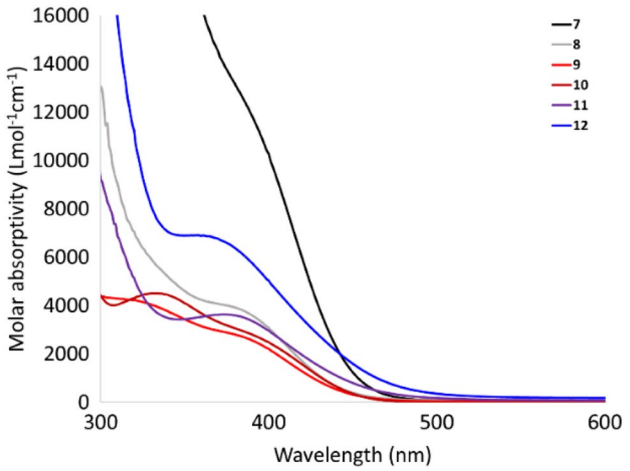

Fig. 2 UV/Vis absorption spectra of complexes **7**–**12** in DMSO

Table 1 Absorbance maxima (λ_{max}, nm) and molar extinction coefficients (ε_{max}, L mol^{-1} cm^{-1}) of the lowest energy transitions in compounds **7–12** in DMSO and CH_2Cl_2

Compounds	DMSO		CH_2Cl_2	
	λ_{max} (nm)	ε_{max} (L mol^{-1} cm^{-1})	λ_{max} (nm)	ε_{max} (L mol^{-1} cm^{-1})
7	380	13,154	311	6116
			390	2078
8	377	3977	380	3582
9	321	4220	331	10,066
	381	2787	385	6860
10	333	4514	339	9619
	393	2718	385	6861
11	376	3640	379	2513
12	362	6906	364	4160

steric crowding around the metal center in the case of the diisopropyl compound [27].

CO release properties

The UV/Vis absorption spectra of **7–12** were registered in two solvents (DMSO and CH_2Cl_2). As shown in Fig. 2, for methoxy (**7**, **8**) and nitro (**11**, **12**) compounds, a broad maximum centred in the range of 362–380 nm is observed in the case of DMSO. Complexes **9** and **10**, incorporating chloride appendage, exhibit two transitions at (321, 381) and (333, 393) nm, respectively (Table 1). There is no systematic shift in the position of the lowest energy transition by changing the character of the substituent in either the *ortho*- or the *para*-position on the phenyl ring (Table 1). On making a comparison between the lowest energy transitions of the complexes, bearing the same substituent at two different positions, we noticed a red-shift behaviour on moving from the *para*- to *ortho*-position clearly seen in the case of the nitro derivatives (**11** and **12**).

To understand the nature of the electronic movement observed in the absorption spectra of **7–12** and how the nature of the substituent in the *ortho*- or *para*-position affects the energies of the MLCT transitions of **7–12**, time-dependent functional theory (TDDFT) calculations were performed using the local minimum structures of the complexes obtained at CAM-B3LYP [31]/GenECP/SMD (LANL2DZ [32] for Br^-, 6-31G(d) for the rest of elements and SMD is the solvation model [33]) level of theory.

Geometry optimizations of **7–12**, in the ground state, were executed at B3LYP [34, 35]/GenECP/SMD level of theory. The starting coordinates for the optimization runs were made based on the obtained crystallographic data. The local minimum structures are shown in Fig. S8. The first 30 singlet excited states were considered in the calculations. The TDDFT spectra of **7–12** are shown in Fig. S9, and the selected transitions with their assignments are given in Table S3. For *para*-substituted derivatives, the transition of interest is HOMO → LUMO + 2, which is found at around 392 nm in all the three *para*-complexes (**8**, **10** and **12**). Based on the TDDFT calculations, it seems that the *para*-substituent has no effect on determining the position of the band at 392 nm in agreement with the experimental finding. As shown in Fig. S10, the HOMO → LUMO + 2 transition has a ground state composed of d(Mn)/p(Br)/π(ligand) and excited state of d(Mn)/p(Br)/π^*(Mn–CO). Thus, the transition at 392 nm may be a combination of d–d/LMCT/MLCT. For the *ortho*-functionalized compounds with $–OCH_3$ (**7**) and –Cl (**9**) groups, the HOMO → LUMO + 2 transition is slightly shifted to 388 nm. As shown in Fig. 3, the transition of interest in **7** originates from the occupied orbital primarily composed of d(Mn)/p(Br)/π(Phenyl) and terminates in LUMO + 2 predominantly made up of π^*(Phenyl) suggesting a nature of MLCT/π–π^* for that transition. For **9**, both the HOMO and LUMO + 2 orbitals are composed of d(Mn), p(Br), and π(phenyl) characters and consequently the transition at 388 nm has d–d/LMCT/MLCT nature. Complex **11**, incorporating a nitro group in the *ortho*-position, has a unique spectrum comprising of several transitions in the range of 390–500 nm. As shown in Fig. 3, the transitions at 397 nm (HOMO–3 → LUMO + 1) and 405 nm (HOMO → LUMO + 2) have characters of MLCT/LMCT and π–π^*, respectively. Based on the TDDFT data, there is no marked change in the wavelength of the lowest energy transitions with the change the type and position of the substituent on the phenyl residue that may be accounted to the main contribution of p(Br) orbital in the character of the lowest energy transition and/or contribution of d–d character to the selected transition.

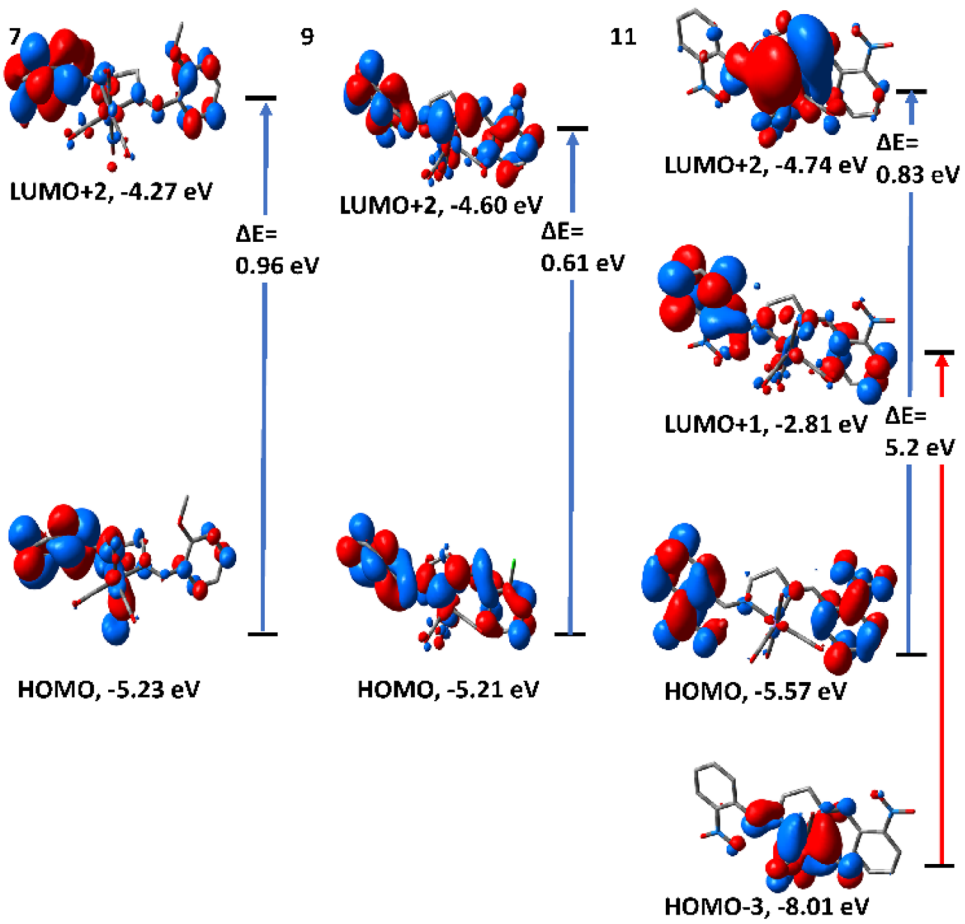

Fig. 3 Selected frontiers molecular orbitals of *ortho*-substituted PhotoCORMs (**7**, **9** and **11**) calculated at CAM-B3LYP/GenECP/SMD (LANL2DZ for Br^-, 6-31G(d) for the rest of elements and SMD is the solvation model) level of theory

The dark stability test of **7–12,** one of the prerequisites for the PhotoCORMs in the phototherapeutic CO applications, in DMSO, was carried out by collecting the UV/Vis spectra over 16 h. Following the incubation period, the compounds were directly exposed to light source at 365 nm (UVIlite LF-206LS, 6 W, UVItec Ltd, Cambridge, UK). Compounds **9**–**12**, bearing electron withdrawing functional group (Cl and NO_2), except the *o*-NO_2 derivative (**11**), demonstrated a major change in intensity of the lowest energy transition (Fig. S11) over the incubation period, while compounds **7** and **8,** incorporating methoxy group, exhibited a minor spectral change (Fig. S12) in the dark under similar experimental conditions. To explore the dark incubation process, the stability test was repeated by collecting the UV/Vis spectra of **7–12** in presence of an excess of sodium bromide. The spectral changes over the incubation period have been significantly reduced in the case of the *p*-Cl derivative (**10**) (Fig. S13). The suppression of the spectral change by the addition of the bromide salt supports the fact that the spectral fluctuation of the dark test may be attributed to the replacement of the axial bromo ligand with the coordinating solvent molecules [18]. Alternatively, the exchange processes in the case of **9** and **12** were faster than in the case of **10** and had not been stopped by addition of bromide salt. To rule out the decomposition of the Mn(I) compounds upon the dissolution in DMSO, the dark stability of some representative compounds of **7–12** in DMSO was followed by IR measurements (*vide infra*). The photolysis profiles of **7** (Fig. S14) and **8** (Fig. 4), bearing methoxy group in the *ortho*- and *para*-positions, respectively, in DMSO, at 365 nm are similar showing a gradual decrease in the intensities of the lowest energy transitions at 380 and 377 nm, in that order. A comparison of the irradiation profiles shows that while *ortho*-methoxy substituted derivative **7** needs 20 min to attain a plateau, the *para*-analogue **8** reaches this final state after longer time of exposure, 25 min. Compound **11,** featuring a nitro group in the *ortho*-position on the phenyl ring, behaved similarly to the methoxy derivatives (**7** and **8**) upon the illumination, and required 15 min to reach the plateau (Fig. S15).

Illumination of **10**, with *p*-Cl group, induced a decrease in the main absorption transitions at 333 and 393 nm (Fig. 5) and the plateau was reached after 10 min of the illumination time. Therefore, while *p*-OCH_3 compound needs 25 min to attain the final stage of the photolysis process, the *p*-Cl derivative reaches this stage already after 10 min indicating

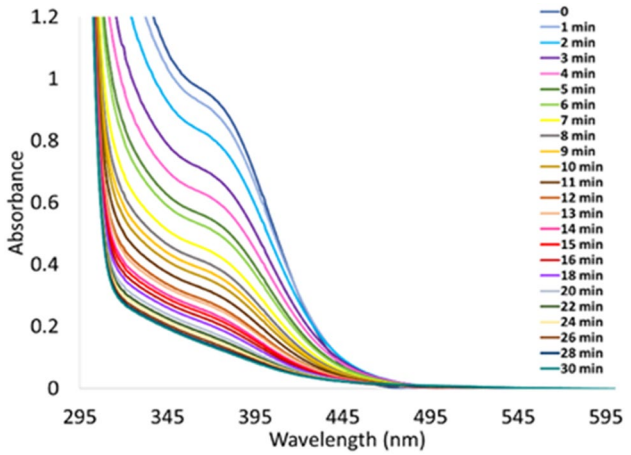

Fig. 4 UV/Vis spectral changes of **8** (0.24 mM in DMSO) upon photolysis at 365 nm with increasing irradiation time (0–30 min)

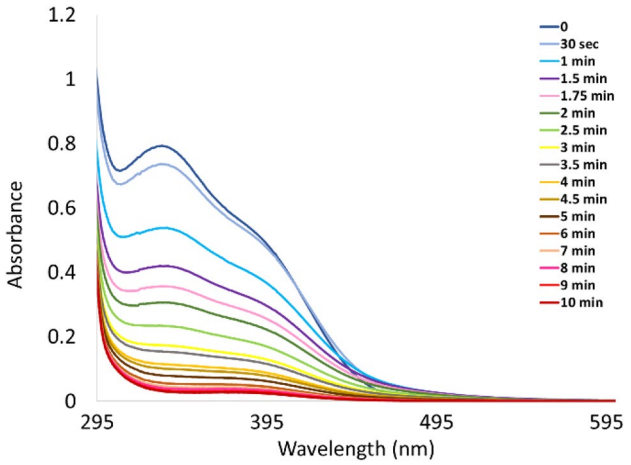

Fig. 5 UV/Vis spectral changes of **10** (0.1 mM in DMSO with tenfold excess of NaBr) upon photolysis at 365 nm with increasing irradiation time (0–10 min)

that the photo process is faster when the compound is functionalized with an electron-withdrawing group.

To get an insight into the dark incubation process and the role of the coordinating solvent in the photolysis kinetics of Mn(I) compounds, we repeated the later studies in a non-coordinating solvent, CH_2Cl_2. Compounds **7**–**12** showed a broad transition in the range of 364–390 nm in CH_2Cl_2 (Fig. 6) with molar absorptivity values of about 2078–6860 L mol^{-1} cm^{-1}. Complexes **7**, **9**, and **10** showed an additional transition at 311, 331, and 339 nm, respectively. The intensities of the lowest energy bands are higher for the electron-withdrawing derivatives (**9**–**12**) than the electron-donating complexes. The compounds show less variation with changing the character of the *para*-substituent. The lowest energy transition of **7**, incorporating *ortho*-methoxy group, is observed at

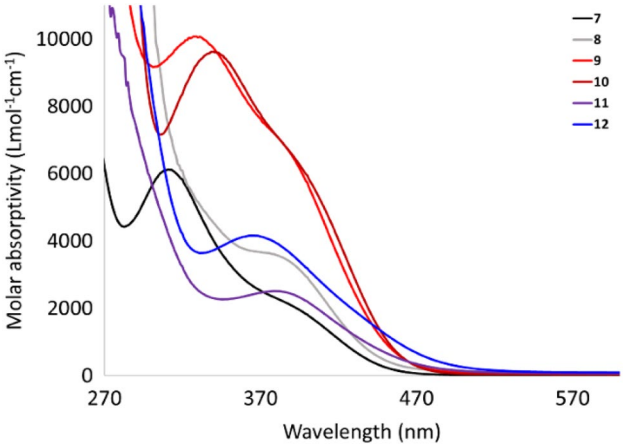

Fig. 6 Electronic absorption spectra of **7–12** in dichloromethane

longer wavelength compared to the rest of the compounds. Switching the position of the OCH_3 and NO_2 groups from the *para* to *ortho* caused a shift in the lowest energy transition towards longer wavelengths. On the other hand, the red shift of the lowest energy transition in **7**–**12** by changing a highly polar solvent, DMSO with a solvent of less polarity, CH_2Cl_2 may be attributed to the negative solvatochromism [36, 37]; a common solvent effect usually observed in the case of some metal carbonyl complexes [37, 38]. Interestingly, the solutions of **7**–**12** in CH_2Cl_2 are stable in the dark for 16 h revealing that the dark process in the case of DMSO may be attributed to a solvent exchange of the bromo ligand and the spectral fluctuations occurred because of the contribution of the p(Br) orbital to the character of the lowest energy transition (HOMO → LUMO + 2) as previously discussed.

When a pre-incubated solution of **7**, in CH_2Cl_2, is exposed to the light source, the intensity of the band at around 390 nm decreases and the plateau level is attained after about 18 min (Fig. 7). Illumination of **8**–**12** (Fig. S16) has a similar effect to **7**, where a decrease in the absorption band(s) with the irradiation time is observed. The plateau values were reached after 9–15 min of the illumination. A comparison of the illumination profiles shows that while *o*-Cl and *o*-NO_2 derivatives (**9** and **11**) need about 15 and 10 min to reach the plateau, the *para*-analogues (**10** and **12**) attain this final state after shorter time of exposure, 10 and 9 min, respectively. This conclusion is *vice versa* with respect to the data obtained in the coordinating solvent revealing that both the solvent and phenyl substituent play important roles in controlling the photoinduced CO release kinetics. Curiously, the investigated compounds released CO in dichloromethane faster than in DMSO as the exchange of the bromo ligand with σ-donor DMSO caused a strengthening of the *fac*-$Mn(CO)_3$ unit.

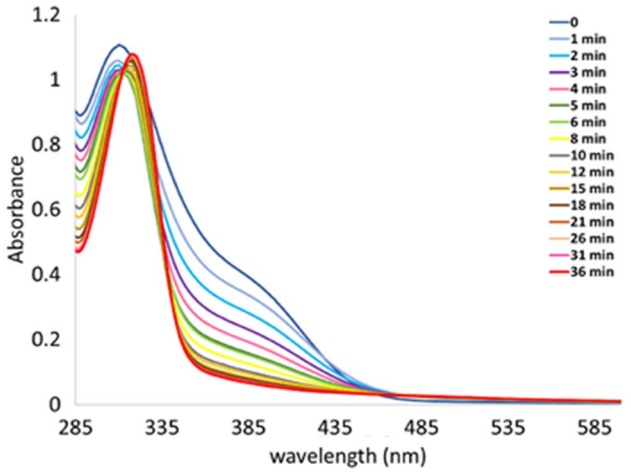

Fig. 7 UV/Vis spectral changes of **7** (0.16 mM in CH_2Cl_2) upon photolysis at 365 nm with increasing illumination time (0–36 min)

IR spectroscopy

To explore the effect of both the character and position of the substituent on the stability and the potential of these *fac*-$Mn(CO)_3$ based compounds to act as PhotoCORMs, solution IR studies were executed using solutions of **8**, **9**, and **11**, in DMSO as representative examples. IR spectra were registered during the photolysis course using identical setup as previously shown in the UV/Vis section. Initially, compounds **9** and **11** were selected to explore the stability in the dark by incubating the solutions for about 5 h, where the incubation stage was interrupted in regular intervals to record the IR spectra (Fig. S17). We did not notice any evidences for the creation of the photo triggered dicarbonyl species or *fac-mer* isomerization in the dark incubation step clearly confirming the stability of the solutions in DMSO as CO photo releasers [39, 40]. The IR spectra of **8**, **9**, and **11** show a sharp symmetrical ν(C≡O) mode of vibration in the range 2017–2019 cm^{-1}, and two anti-symmetric ν(C≡O) bands at 1916–1930, and 1898–1912 cm^{-1} [39]. Previous spectroscopic and DFT studies showed that only one CO ligand is photolytically liberated from the coordination sphere of the tricarbonyl Mn(I) complexes, while the rest of CO molecules require an additional dark process [39, 41]. Upon the irradiation, the intensities of the ν(C≡O) bands of **8** decreased gradually accompanied by growing of a new band of low intensity at 1849 cm^{-1}, which is assigned to *cis*-$Mn(CO)_2$ species [18, 42, 43]. As shown in Fig. 8, the second band of the dicarbonyl species was visualized at about 1934 cm^{-1}. Since *cis*-$Mn(CO)_2$ intermediate is photolabile, the characteristic ν(C≡O) bands disappeared after prolonged illumination. Conversion of *fac*-$Mn(CO)_3$ into the dicarbonyl species, as a function of the illumination time is clearly seen by monitoring the grown of the band at 1866 cm^{-1} in the case of **9** (Fig. S18). In compound **11** (Fig. S18), incorporating *o*-NO_2 group, the kinetics of the CO release was faster than in the cases of **8** and **9** and thus it was not possible to trap the intermediate species [41]. Based on the IR investigation, the solutions of the representative compounds are stable in DMSO in the dark, and the investigated PhotoCORMs are capable of releasing CO upon the exposure to light source at 365 nm.

Cell viability assay

The cytotoxicity of the ligands **1–6** and their PhotoCORMs **7–12**, with and without illumination, was evaluated by incubating the cell cultures of HepG2 with the synthesized compounds at different concentrations (5–50 µM). The cell cultures, treated with the compounds, were kept in the dark for 2 h. A similar set of the cells was prepared, treated with

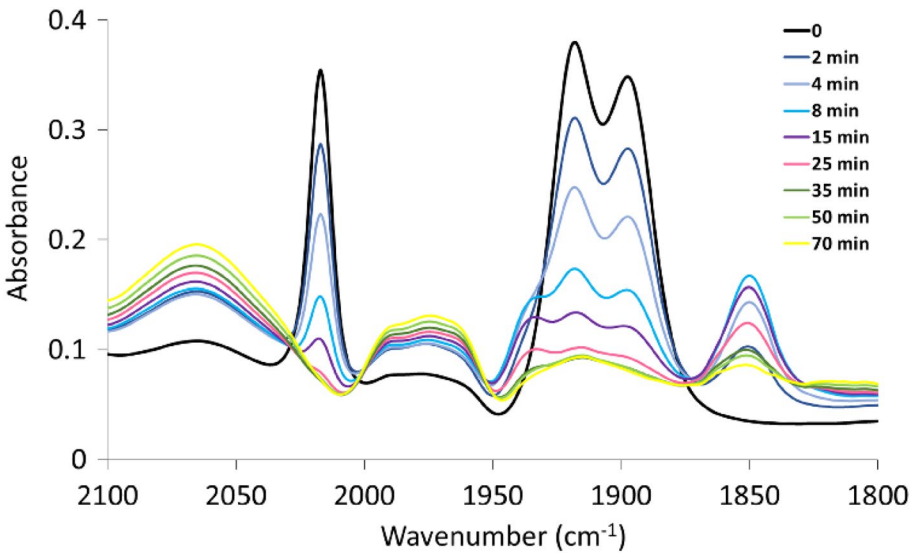

Fig. 8 IR spectral changes of complex **8** (8 mM) upon illumination with a 365 nm light for 70 min

the same compounds, and then illuminated for 45 min. Control experiments including DMSO and medium were conducted in the dark and upon the irradiation. The viability of HepG2 cells was assessed by MTT assay. Neither the medium nor the solvent has a significant effect on the cell viability even after the irradiation at 365 nm for 45 min. As shown in Fig. 9, the free ligands (**1–6**) and nitro-functionalized compounds (**11** and **12**) are non-toxic to HepG2 cells up to 50 µM under both the dark and illumination conditions.

In the dark, compounds **7** and **9**, incorporating *o*-OCH_3 and *o*-Cl, exhibit excellent cytotoxicity with IC_{50} values of 18.1 and 11.8 µM, respectively, while their *para*-analogues (**8** and **10**) are inactive up to 50 µM (Table 2). Upon the irradiation, complexes **7** and **9** became more toxic, where

Table 2 IC_{50} values of complexes **7**–**12** against HepG2 cells in the dark and upon the exposure to the light source

Compounds	IC_{50} values (µM)	
	Non-irradiated	Irradiated
7	18.1	7.9
8	> 50	5.7
9	11.8	6.6
10	> 50	6.7
11	> 50	> 50
12	> 50	> 50

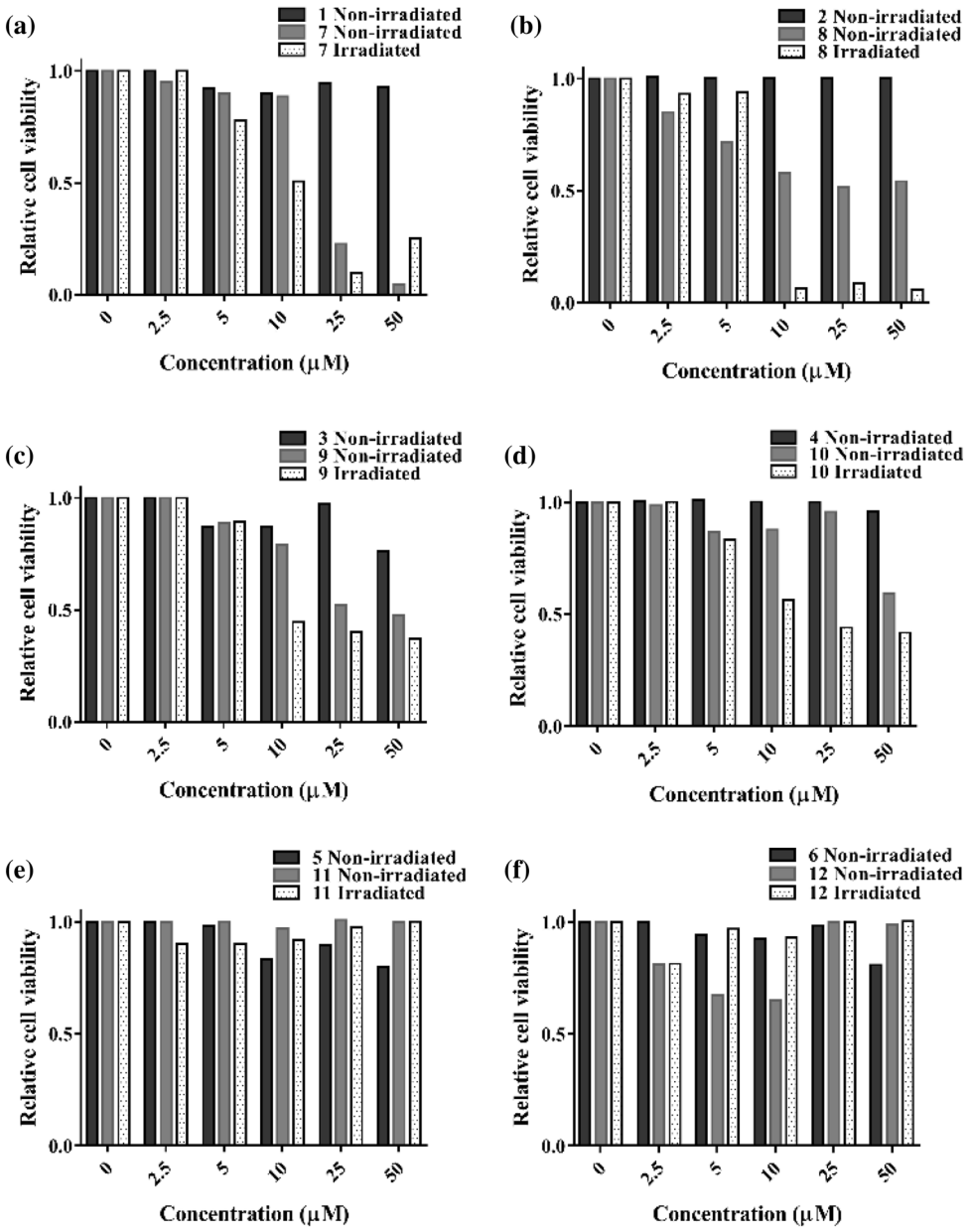

Fig. 9 The cytotoxic activity of the free ligands (**1–6**) and PhotoCORMs (**7**–**12**) against HepG2 cells using MTT assay with and without illumination for 45 min at different concentrations (0–50 µM)

the IC_{50} values decreased to 7.9 and 6.6 μM, in that order. When the inactive compounds **8** and **10** exposed to the light source, a significant cytotoxicity to HepG2 was developed with IC_{50} values of 5.7 and 6.7 μM. On the other hand, the inactivity of the nitro compounds **11** and **12** does not change upon the illumination. The cytotoxicity of the illuminated compounds was found to be in the following order *p*-OCH_3 (**8**) > *o*- and *p*-Cl (**9**, **10**) > *o*-OCH_3 (**7**). The developed antiproliferative activities of **8** and **10** as well as the improvement of the cytotoxicity of **7** and **9** may be attributed the nature of the iCORM and is not due to the influence of CO alone [44]. This conclusion was presumed based on the inactivity of the nitro derivatives before and after illumination, which implemented the absence of the role of CO alone in the antiproliferative activity of our compounds. To date, Zobi and co-workers concluded that the developed cytotoxicity against A549 and HT29 cells of some [$MnBr(CO)_3L$] (L: ethynyl-α-diimine ligands) and their cobalamin conjugates, upon illumination, may be attributed to both CO and iCORM [44]. It was unclear how the CO sensitize the the malignant cells to iCORM. In comparison, PhotoCORM **8**, incorporating *p*-OCH_3, displays the highest antiproliferative activity upon illumination, making it the most phototoxic complex in our study, while compound **7**, bearing *o*-OCH_3, is an interesting compound attributable to its toxicity, with and without illumination. Thus, greatest potential, for further investigations of the methoxy derivatives and the nature of the developed photo cytotoxicity (e.g. synergetic effect) is highly recommended.

Conclusion

Six bromo tricarbonyl Mn(I) complexes of *N,N*-bidentate ligands decorated with different electron-withdrawing and electron-donating substituents (R=OCH_3, Cl, and NO_2) in the *ortho*- and *para*-positions on the phenyl residue were synthesized, and fully characterized including X-ray crystallographic analysis for four complexes. The phenyl substituent played a vital role in determining the dark stability of Mn(I) complexes, one of the prerequisites for the compounds to be investigated as potential CO releasers in the CO phototherapeutic applications. Time-dependent density functional theory calculations indicated the contribution of p(Br) orbital in the composition of the lowest energy transitions. In DMSO, a coordinating solvent, we noticed a major spectral change in the intensity of the MLCT band in the case of some compounds bearing electron-withdrawing groups, which was suppressed by addition of bromide salt in some cases. For compounds incorporating electron-donating group, e.g. OCH_3, the spectral fluctuation was negligible. The dark stability step was investigated by solution IR studies. We did not notice any evidences for the creation of the photo induced dicarbonyl species or *fac-mer* isomerization confirming the stability of the solutions of the CO photo releasers in DMSO. Besides, we repeated the dark stability test in a non-coordinating solvent e.g. CH_2Cl_2. No spectral fluctuations were observed even for the compounds bearing electron-withdrawing group. We deduced a probability of exchange of the axial bromo ligand with DMSO molecules. The solvent dependence was manifested by the red shift of MLCT observed on switching from a high polar solvent to a low polar one, which may be attributed to the negative solvatochromism.

Release of carbon monoxide from the investigated PhotoCORMs was investigated by solution IR and UV/Vis spectroscopy. All the title complexes exhibited a rather similar photolysis profiles and attained values after about 10–30 min of exposure to 365 nm. The compounds released CO in dichloromethane faster than in DMSO as the exchange of the bromo ligand with σ-donor DMSO caused a strengthening of the *fac*-$Mn(CO)_3$ unit. Both the phenyl substituent (character and position) and the coordinating ability of the solvent played important roles in controlling the CO release kinetics. In DMSO, IR spectroscopic investigations revealed that the CO release is a stepwise process that takes place via the formation of the photoactive *cis*-$Mn(CO)_2$ intermediate.

The cytotoxicity of the free ligands and their PhotoCORMs, with and without illumination, was evaluated against the malignant HepG2 cells. The free ligands and nitro-compounds are non-cytotoxic to HepG2 cells up to 50 μM under both the dark and illumination conditions. In the dark, compounds bearing *o*-OCH_3 and *o*-Cl exhibit excellent cytotoxicity with IC_{50} values of 18.1 and 11.8 μM, respectively, while their *para*-analogues are inactive. Upon illumination, the cytotoxic activity of the latter mentioned compounds increased and the inactive compounds became active. The developed cytotoxicity may be allocated for the iCORM (residue after CO release) or synergetic effect (CO and iCORM) [44]. This conclusion is based on the inactivity of the nitro derivatives even after the release of the CO molecules. Finally, the *p*-OCH_3 compound displayed the highest antiproliferative activity upon illumination, making it the most phototoxic complex in our study, while the *o*-OCH_3 is an interesting compound attributable to its toxicity in the dark and upon illumination and thus greatest potential, for further investigations is highly recommended for methoxy derivatives.

Experimental section

Materials and instruments

Ethylenediamine, *ortho*- and *para*-substituted benzaldehydes (R=OCH_3, Cl, and NO_2), bromo pentacarbonyl

manganese(I), and organic solvents were purchased from the commercial sources and used without preliminary purifications. Solid-state IR spectra were recorded on a JASCO FT/IR-4100 instrument and a Nicolet 380 FT-IR spectrometer equipped with a smart iFTR accessory. ^{1}H and $^{13}C\{^{1}H\}$ NMR spectra were run on Bruker-Advance 400 (^{1}H, 400.40 MHz; $^{13}C(^{1}H)$, 100.70 MHz) spectrometer. Electrospray ionization mass spectra, were recorded with an Advion compact mass spectrometer. Automatic Analyzer CHNS, Vario EL III Elementar, a Vario Micro Cube analyzer of Elementar Analysensysteme and an EA 3000 elemental analyzer from HEKtech were used to determine the micro-elemental percentages of the studied complexes. UV/Vis spectra were recorded by a Specord 210 Plus spectrophotometer.

Synthetic procedures

Synthesis of ligands (1–6)

Compounds **1–6** were synthesized according to a modified literature method [45, 46] via the condensation of ethylenediamine with two equivalents of *ortho*- and *para*-substituted benzaldehydes, R=OCH_3, Cl and NO_2, in anhydrous ethanol for 2 h. White to yellow powders formed upon the slow evaporation of the solvent from the reaction mixtures of **1–5**, which were washed with diethyl ether and dried under vacuum. For **6**, precipitation occurred during the reflux and the product was collected by filtration, washed with ethanol, diethyl ether and then dried.

1 (R=2-OCH_3). Yellow powder, yield: 21% (600 mg, 2.02 mmol). IR (ATR, cm^{-1}): $\nu = 2926$ (CH), 2897 (CH), 2841 (CH), 1632, 1285, 1242, 1016. ^{1}HNMR ([D_6] DMSO, 400.40 MHz): $\delta = 8.61$ (s, 1H, HC=N), 7.79 (dd, $^{3}J_{H,H=}$5.91 Hz, $^{4}J_{H,H=}$1.77 Hz, 1H, Ph-H6), 7.40 (td, $^{3}J_{H,H=}$7.21 Hz, $^{3}J_{H,H=}$1.94 Hz, 1H, Ph-H4), 7.05 (d, $^{3}J_{H,H=}$8.19 Hz, 1H, Ph-H3), 6.96 (t, $^{3}J_{H,H=}$7.77 Hz, 1H, Ph-H5), 3.84 (s, 2H, CH_2), 3.78 (s, 3H, CH_3) ppm. ^{13}C NMR ([D_6] DMSO, 100.63 MHz): $\delta = 158.3$, 157.1, 132.0, 126.6, 124.0, 120.4, 111.8, 61.3 (CH_3), 55.5 (CH_2) ppm. $C_{18}H_{20}N_2O_2$: C 72.95, H 6.80, N 9.45; found C 72.70, H 6.86, N 9.66.

2 (R=4-OCH_3). Yellow powder, yield: 18% (690 mg, 2.32 mmol). IR (ATR, cm^{-1}): $\nu = 2919$ (CH), 2842 (CH), 1639, 1602, 1508, 1281, 1248, 1017. ^{1}HNMR ([D_6] DMSO, 400.40 MHz): $\delta = 8.24$ (s, 1H, HC=N), 7.64 (d, $^{3}J_{H,H=}$8.76 Hz, 2H, Ph-H2/H6), 6.96 (d, $^{3}J_{H,H=}$8.73 Hz, 2H, Ph-H3/H5), 3.80 (s, 2H, CH_2), 3.78 (s, 3H, CH_3) ppm. ^{13}C NMR ([D_6] DMSO, 100.63 MHz): $\delta = 161.1$, 161.0, 129.3, 128.9, 114.0, 61.0 (CH_3), 55.2 (CH_2) ppm. $C_{18}H_{20}N_2O_2$: C 72.95, H 6.80, N 9.45; found C 72.61, H 7.01, N 10.29.

3 (R=2-Cl). White powder, yield: 21% (808 mg, 2.65 mmol). IR (ATR, cm^{-1}): $\nu = 2919$ (CH), 2898 (CH), 2855 (CH), 1630, 1592, 1567, 1015, 966. ^{1}HNMR ([D_6] DMSO, 400.40 MHz): $\delta = 8.64$ (s, 1H, HC=N), 7.93 (d, $^{3}J_{H,H=}$6.17 Hz, 1H, Ph-H6), 7.47 (m, 2H, Ph-H3/H4), 7.38 (t, $^{3}J_{H,H=}$6.27 Hz, 1H, Ph-H5), 3.95 (s, 2H, CH_2) ppm. ^{13}C NMR ([D_6] DMSO, 100.63 MHz): $\delta = 158.4$, 133.9, 132.6, 132.1, 129.8, 128.0, 127.4, 60.4 (CH_2) ppm. $C_{16}H_{14}Cl_2N_2$: C 62.97, H 4.62, N 9.18; found C 63.03, H 4.52, N 9.35.

4 (R=4-Cl). White powder, yield: 16% (447 mg, 1.46 mmol). IR (ATR, cm^{-1}): $\nu = 2920$ (CH), 2861 (CH), 1642, 1594, 1485, 1014, 703. ^{1}HNMR ([D_6] DMSO, 400.40 MHz): $\delta = 8.33$ (s, 1H, HC=N), 7.72 (d, $^{3}J_{H,H=}$8.49 Hz, 2H, Ph-H2/H6), 7.48 (d, $^{3}J_{H,H=}$8.59 Hz, 2H, Ph-H3/H5), 3.87 (s, 2H, CH_2) ppm. ^{13}C NMR ([D_6] DMSO, 100.63 MHz): $\delta = 158.6$, 132.9, 132.6, 127.2, 126.5, 58.4 (CH_2) ppm. $C_{16}H_{14}Cl_2N_2$: C 62.97, H 4.62, N 9.18; found C 63.17, H 5.24, N 9.34.

5 (R=2-NO_2). Yellow powder, yield: 52.0% (1048 mg, 3.21 mmol). IR (ATR, cm^{-1}): $\nu = 3103$ (CH), 3052 (CH), 2917 (CH), 1636, 1512, 1335, 1017. ^{1}HNMR ([D_6] DMSO, 400.40 MHz): $\delta = 8.58$ (s, 1H, HC=N), 7.99 (dd, $^{3}J_{H,H=}$8.05 Hz, $^{4}J_{H,H=}$1.24 Hz, 1H, Ph-H6), 7.96 (dd, $^{3}J_{H,H=}$7.75 Hz, $^{4}J_{H,H=}$1.30 Hz, 1H, Ph-H4), 7.76 (td, $^{3}J_{H,H=}$7.45 Hz, $^{4}J_{H,H=}$1.05 Hz, 1H, Ph-H3), 7.68 (td, $^{3}J_{H,H=}$8.02 Hz, $^{4}J_{H,H=}$1.64 Hz, 1H, Ph-H5), 3.94 (s, 2H, CH_2) ppm. ^{13}C NMR ([D_6] DMSO, 100.63 MHz): $\delta = 158.2$, 148.8, 133.4, 131.2, 129.9, 129.4, 124.1, 60.6 (CH_2) ppm. $C_{16}H_{14}N_4O_4$: C 58.89, H 4.32, N 17.17; found C 59.31, H 4.95, N 17.39.

6 (R=4-NO_2). Orange powder, yield: 35% (1218 mg, 3.73 mmol). IR (ATR, cm^{-1}): $\nu = 3100$ (CH), 2911 (CH), 2885 (CH), 2855 (CH), 1645, 1515, 1335, 1016. ^{1}HNMR ([D_6] DMSO, 400.40 MHz): 8.51 (s, 1H, HC=N), 8.27 (d, $^{3}J_{H,H=}$8.97 Hz, 2H, Ph-H3/H5), 7.97 (d, $^{3}J_{H,H=}$8.86 Hz, 2H, Ph-H2/H6), 3.99 (s, 2H, CH_2) ppm. ^{13}C NMR ([D_6] DMSO, 100.63 MHz): $\delta = 160.7$, 148.5, 141.5, 128.8, 123.9, 60.7 (CH_2) ppm. $C_{16}H_{14}N_4O_4$:C 58.89, H 4.32, N 17.17; found C 59.00, H 4.63, N 17.61.

Synthesis of tricarbonyl manganese(I) complexes (7–12)

Schiff-base (SB) ligands (**1**–**6**) [0.18 mmol; 53 mg (**1**, **2**), 55 mg (**3**, **4**) and 58.6 mg (**5**, **6**)] and [$MnBr(CO)_5$] (0.18 mmol; 50 mg) were dissolved in chloroform (10 mL) and then the reaction mixtures were heated to reflux in the dark for 3 h. The precipitates were collected by filtration, washed with diethyl ether (3 × 5 mL) and then dried under vacuum.

7: [$MnBr(CO)_3$(SB-2OCH_3)]. Yellow powder, yield: 39% (36 mg, 0.069 mmol). IR (ATR, cm^{-1}): $\nu = 2937$ (CH), 2841 (CH), 2018 (vs, C≡O), 1908 (vs, C≡O), 1622, 1295, 1252, 1020. ^{1}HNMR ([D_6] DMSO, 400.40 MHz): $\delta = 9.13$ (s, 1H, HC=N), 9.07 (s, 1H, HC=N), 7.81 (d, $^{3}J_{H,H=}$1.94 Hz, 1H, Ph-H6), 7.57 (m, 3H, Ph-H4/H6),

7.19 (m, 4H, Ph-H3/H5), 4.07 (m, 4H, CH_2), 3.90 (m, 6H, CH_3) ppm. ESI–MS (positive mode, acetone): $m/z = 434.9$ $[M–Br]^+$, 351.0 $[M–Br–3CO]^+$ (M = molecular mass). $C_{21}H_{20}BrMnN_2O_5{\cdot}2H_2O$: C 45.75, H 4.39, N 5.08; found C 46.19, H 4.17, N 4.94.

8: [$MnBr(CO)_3$(SB-4OCH_3)]. Orange powder, yield: 49% (45 mg, 0.088 mmol). IR (ATR, cm^{-1}): $\nu = 2931$ (CH), 2839 (CH), 2018 (vs, C≡O), 1908 (vs, C≡O), 1604, 1260, 1026. ^{1}HNMR ([D_6] DMSO, 400.40 MHz): $\delta = 9.11$ (br, 1H, HC=N), 8.96 (br, 1H, HC=N), (7.96, 7.76) (br, 4H, Ph-H2/H6), 7.12 (br, 4H, Ph-H3/H5), 3.85 (br, 10H, CH_2/CH_3) ppm. $C_{21}H_{20}BrMnN_2O_5{\cdot}H_2O{\cdot}CHCl_3$: C 40.52, H 3.53, 4.29; found C 40.45, H 3.72, N 4.42.

9: [$MnBr(CO)_3$(SB-2Cl)]. Yellow powder, yield 66% (62 mg, 0.12 mmol). IR (ATR, cm^{-1}): $\nu = 3053$ (CH), 2925 (CH), 2016 (vs, C≡O), 1905 (vs, C≡O), 1627, 1042, 754. ^{1}HNMR ([D_6] DMSO, 400.40 MHz): $\delta = 9.25$ (s, 2H, HC=N), 7.76 (d, 2H, Ph-H6), 7.51–7.49 (m, 6H, Ph-H3/H4/H5), 4.35 (m, 2H, CH_2), 4.06 (m, 2H, CH_2) ppm. ^{13}C NMR ([D_6] DMSO, 100.63 MHz): $\delta = 173.2$, 158.9, 135.6, 132.5, 130.5, 129.7, 127.7, 63.0 ppm. ESI–MS (positive mode, acetone): $m/z = 443.3$ $[M–Br]^+$, 359.2 $[M–Br–3CO]^+$. $C_{19}H_{14}BrMnN_2O_3Cl_2$: C 43.54, H 2.69, N 5.35; found C 43.04, H 2.88, N 5.61.

10: [$MnBr(CO)_3$(SB-4Cl)]. Orange powder, yield 55% (63 mg, 0.12 mmol). IR (ATR, cm^{-1}): $\nu = 2925$ (CH), 2022 (vs, C≡O), 1905 (vs, C≡O), 1628, 1088, 680. ^{1}HNMR ([D_6] DMSO, 400.40 MHz): $\delta = 9.23$ (s, 1H, HC=N), 9.12 (s, 1H, HC=N), 7.86–7.50 (m, 8H, Ph-H3/H4/H5/H6), 4.10–3.99 (m, 4H, CH_2) ppm. ^{13}C NMR ([D_6] DMSO, 100.63 MHz): $\delta = 174.9$, 169.6, 161.3, 136.7, 135.8, 135.3, 132.1, 131.5, 130.8, 130.5, 129.9, 129.4, 129.2, 129.0, 64.3 and 55.1 ppm. ESI–MS (negative mode, acetone): $m/z = 544.4$ $[M + Br–2CO]^-$. $C_{19}H_{14}BrMnN_2O_3Cl_2{\cdot}H_2O{\cdot}0.5CHCl_3$: C 39.02, H 2.75, N 4.66; found C 38.94, H 2.70, N 5.11.

11: [$MnBr(CO)_3$(SB-2NO_2)]. Orange powder, yield: 50% (49 mg, 0.091 mmol). IR (ATR, cm^{-1}): $\nu = 2926$ (CH), 2856 (CH), 2021 (vs, C≡O), 1937 (sh, C≡O), 1902 (vs, C≡O), 1643, 1521, 1342, 1046. ^{1}HNMR ([D_6] DMSO, 400.40 MHz): $\delta = 9.45$ (s, 1H, HC=N), 8.35 (br, 1H, Ph-H6), 7.99–7.84 (br, 3H, Ph-H3/H4/H5), 4.36–4.06 (br, 2H, CH_2) ppm. ^{13}C NMR ([D_6] DMSO, 100.63 MHz): $\delta = 173.0$, 146.4, 135.5, 132.5, 132.2, 130.9, 125.0, 62.8 ppm. ESI–MS (positive mode, acetone): $m/z = 464.9$ $[M–Br]^+$. $C_{19}H_{14}BrMnN_4O_7{\cdot}2H_2O$: C 39.26, H 3.12, N 9.64; found C 39.64, H 2.92, N 9.90.

12: [$MnBr(CO)_3$(SB-4NO_2)]. Orange powder, yield: 47% (46 mg, 0.084 mmol). IR (ATR, cm^{-1}): $\nu = 2927$ (CH), 2021 (vs, C≡O), 1945 (sh, C≡O), 1912 (vs, C≡O), 1639, 1519, 1350, 1034. ^{1}HNMR ([D_6] DMSO, 400.40 MHz): $\delta = 9.43$ (s, 1H, HC=N), 8.26 (br, 4H), 4.05 (br, 2H, CH_2) ppm. $C_{19}H_{14}BrMnN_4O_7{\cdot}CHCl_3$: C 36.15, H 2.28, N 8.43; found C 35.84, H 2.55, N 8.74.

Single crystal X-ray diffraction analysis

Single crystals of compounds **7**, **8, 10** and **11**, appropriate for X-ray diffraction analysis, were grown by diffusion of *n*-hexane into the solutions of the tricarbonyl manganese(I) complexes in dichloromethane. Diffraction data of the compounds were collected on a RIGAKU OXFORD DIFFRACTION XtaLAB Synergy diffractometer with a semiconductor HPA-detector (HyPix-6000) and multi-layer mirror monochromated $Cu–K_\alpha$ radiation at 100 K. The structures of tricarbonyl Mn(I) complexes were solved using the intrinsic phasing method (SHELXT program) [47], and refined with a full-matrix least-squares procedure using SHELXL program [48] and the SHELXLE graphical user interface [49]. All non-hydrogen atoms were refined in anisotropic approximation, with hydrogen atoms 'riding' on idealised positions. Crystals of **7** and **11** show the disorder of [OC–Mn–Br][Br–Mn–CO] and the solutions of the structures can be considered as a proof of the conformation of the molecule. Crystal data and experimental details are listed in Table S1. Crystallographic data have been deposited with the Cambridge Crystallographic Data Centre as supplementary publication no. CCDC 2032876 (**7**), 2032872 (**8**), 2032874 (**10**) and 2032875 (**11**).

Quantum chemical calculations

DFT and TDDFT calculations were executed using Gaussian03 [50]. The local minimum structures of **7–12** were obtained at B3LYP [34, 35]/GenECP/SMD level of theory (LANL2DZ [32] for Br^-, 6-31G(d) for the rest of elements and SMD is the solvation model [33]). A similar methodology is commonly reported in the literature for the ground-state optimization of other metal-based compounds [51–54]. The electronic transitions were calculated by CAM-B3LYP [31]/GenECP/SMD. Visualization of the ground state optimized structures, Frontier molecular orbitals, and electronic spectra was performed with Gaussview03 [55].

IR spectroscopic studies

A few milliliters of 8 mM solutions of the studied compounds, in DMSO, was injected into a liquid-IR cell, with potassium bromide windows (path length = 0.1 mm). The cell was irradiated with a 365 nm UV lamp. The Irradiation process was interrupted at regular intervals to register the vibrational spectra and the photolysis was terminated when no further changes observed. Bruker Alpha-T spectrometer was used to monitor the dark stability and the spectral changes upon the illumination.

Biological activity

Cell culture The HepG2 cell line (human hepatocarcinoma cell line) was purchased from VACSRA, Egypt and cultured in Dulbecco's modified Eagle's (DMEM) medium supplemented with 10% (v/v) fetal bovine serum, seeded into 96-well plates (1×10^4 cells/well) and incubated for 24 h at 37 °C and 5% of carbon dioxide.

Cell cytotoxicity assay MTT (3-(4,5-dimethylthiazol-2-yl)-2,5-diphenyltetrazolium bromide) assay was used to assess the cytotoxic effect of the free Schiff-base ligands (**1–6**) and their PhotoCORMs (**7–12**) towards HepG2 [56]. The malignant cells were seeded into 96-well plates (1×10^4 cells/well) and incubated for 24 h. The MTT assay was executed in the dark, to avoid the loss of CO upon the exposure to light, and upon the irradiation to explore the effect of CO and iCORM on the malignant cells. Two sets of cells were prepared and incubated in the presence of the same concentration (0–50 µM) of either the free ligand or the complex in the dark for 2 h. The media were aspirated and then the cells were washed with phosphate-buffered saline (PBS). Afterwards, the cells were incubated with fresh media for further 45 min. One of the two sets was exposed to light source at 365 nm at a distance of 3 cm for 45 min. Under the same conditions, two control sets (DMSO and media), at the same concentration used with the PhotoCORMs, were prepared and kept in the dark to investigate the influence of illumination on HepG2 cells. The prepared sets were re-incubated for 3 h for recovery, washed with PBS and then 100 µl of MTT (0.5 mg/mL) was added. Incubation for 4 h was the next stage. To get rid of the formed formazan crystals, 100 µl of DMSO was added. The plates were agitated for 20 min and then the absorbance values were recorded at 392 nm using a microplate reader. The relative cell viability was evaluated by normalizing the absorbance of the treated cells to the control and the untreated cells. The IC_{50} was determined by non-linear regression analysis GraphPad Prism 7.0 software.

Supplementary Information The online version contains supplementary material available at https://doi.org/10.1007/s00775-020-01843-7.

Acknowledgements K.R. thanks Julius-Maximilians-Universität Würzburg for support. A.M., R.K., M.H. and N.A. thank Cairo University for research support.

Compliance with ethical standards

Conflict of interest There are no conflicts to declare.

References

1. Romão CC, Blättler WA, Seixas JD, Bernardes GJ (2012) Chem Soc Rev 41:3571–3583
2. Wegiel B, Gallo D, Csizmadia E, Harris C, Belcher J, Vercellotti GM, Penacho N, Seth P, Sukhatme V, Ahmed A (2013) Cancer Res 73:7009–7021
3. Hartsfield CL (2002) Antioxid Redox Signaling 4:301–307
4. Koçer G, Nasircilar Ülker S, Şentürk ÜK (2018) Microcirculation 25:12495
5. Motterlini R, Clark JE, Foresti R, Sarathchandra P, Mann BE, Green CJ (2002) Circ Res 90:17–24
6. Clark JE, Naughton P, Shurey S, Green CJ, Johnson TR, Mann BE, Foresti R, Motterlini R (2003) Circ Res 93:2–8
7. Ji X, De La Cruz LKC, Pan Z, Chittavong V, Wang B (2017) Chem Commun 53:9628–9631
8. Kueh JTB, Stanley NJ, Hewitt RJ, Woods LM, Larsen L, Harrison JC, Rennison D, Brimble MA, Sammut IA, Larsen DS (2017) Chem Sci 8:5454–5459
9. Stamellou E, Storz D, Botov S, Ntasis E, Wedel J, Sollazzo S, Krämer B, van Son W, Seelen M, Schmalz H (2014) Redox Biol 2:739–748
10. Romanski S, Kraus B, Schatzschneider U, Neudörfl JM, Amslinger S, Schmalz HG (2011) Angew Chem Int Ed 50:2392–2396
11. Schatzschneider U (2015) Br J Pharmacol 172:1638–1650
12. Schatzschneider U (2010) Eur J Inorg Chem 2010:1451–1467
13. Queiroga CS, Vercelli A, Vieira HL (2015) Br J Pharmacol 172:1533–1545
14. Seixas JD, Mukhopadhyay A, Santos-Silva T, Otterbein LE, Gallo DJ, Rodrigues SS, Guerreiro BH, Gonçalves AM, Penacho N, Marques AR (2013) Dalton Trans 42:5985–5998
15. Rimmer RD, Richter H, Ford PC (2010) Inorg Chem 49:1180–1185
16. Mansour AM, Radacki K (2020) Inorg Chim Acta 511:119806
17. Jiang Q, Xia Y, Barrett J, Mikhailovsky A, Wu G, Wang D, Shi P, Ford PC (2019) Inorg Chem 58:11066–11075
18. Mansour AM, Steiger C, Nagel C, Schatzschneider U (2019) Eur J Inorg Chem 2019:4572–4581
19. Mansour AM (2018) Eur J Inorg Chem 2018:4805–4811
20. Mansour AM, Shehab OR (2018) Inorg Chim Acta 480:159–165
21. Mansour AM (2017) Appl Organomet Chem 31:3564
22. Mansour AM, Friedrich A (2017) Inorg Chem Front 4:1517–1524
23. Kottelat E, Ruggi A, Zobi F (2016) Dalton Trans 45:6920–6927
24. Carrington SJ, Chakraborty I, Bernard JM, Mascharak PK (2014) ACS Med Chem Lett 5:1324–1328
25. Gonzalez MA, Carrington SJ, Fry NL, Martinez JL, Mascharak PK (2012) Inorg Chem 51:11930–11940
26. Niesel J, Pinto A, N'Dongo HWP, Merz K, Ott I, Gust R, Schatzschneider U (2008) Chem Commun 2008:1798–1800
27. Yempally V, Kyran SJ, Raju RK, Fan WY, Brothers EN, Darensbourg DJ, Bengali AA (2014) Inorg Chem 53:4081–4088
28. Khaled RM, Friedrich A, Ragheb MA, Abdel-Ghani NT, Mansour AM (2020) Dalton Trans 49:9294–9305
29. Frei A, Zuegg J, Elliott AG, Baker M, Braese S, Brown C, Chen F, Dowson CG, Dujardin G, Jung N (2020) Chem Sci 11:2627–2639
30. Jean-Baptiste KN, Guillaume KC, Landry KA, Claude KMW, Ahoua ARC, Nahosse Z (2017) IRA Int J Appl Sci 6:23–30
31. Hay PJ, Wadt WR (1985) J Chem Phys 82:270–283
32. Wadt WR, Hay PJ (1985) J Chem Phys 82:284–298
33. Marenich AV, Cramer CJ, Truhlar DG (2009) J Phys Chem B 113:6378–6396
34. Raghavachari K (2000) Theor Chem Acc 103:361–363
35. Becke AD (1988) Phys Rev A 38:3098
36. Kianfar E, Apaydin DH, Knör G (2017) ChemPhotoChem 1:378–382
37. Dodsworth ES, Lever A (1990) Inorg Chem 29:499–503
38. Manuta DM, Lees AJ (1986) Inorg Chem 25:3212–3218

39. Nagel C, McLean S, Poole RK, Braunschweig H, Kramer T, Schatzschneider U (2014) Dalton Trans 43:9986–9997
40. Sachs U, Schaper G, Winkler D, Kratzert D, Kurz P (2016) Dalton Trans 45:17464–17473
41. Berends H-M, Kurz P (2012) Inorg Chim Acta 380:141–147
42. Pai S, Hafftlang M, Atongo G, Nagel C, Niesel J, Botov S, Schmalz H-G, Yard B, Schatzschneider U (2014) Dalton Trans 43:8664–8678
43. Ward JS, Lynam JM, Moir JW, Sanin DE, Mountford AP, Fairlamb IJ (2012) Dalton Trans 41:10514–10517
44. Rossier J, Delasoie J, Haeni L, Hauser D, Rothen-Rutishauser B, Zobi F (2020) J Inorg Biochem 209:111122
45. Thirunarayanan G (2014) Bull Chem Soc Ethiop 28:73–79
46. Mirkhani V, Kia R, Vartooni AR, Milic D (2009) Transit Met Chem 34:225–230
47. Sheldrick GM (2015) Acta Crystallogr Sect A Found Adv 71:3–8
48. Sheldrick GM (2008) Acta Crystallogr Sect A Found Crystallogr 64:112–122
49. Hübschle CB, Sheldrick GM, Dittrich B (2011) J Appl Crystallogr 44:1281–1284
50. Frisch MJ, Trucks GW, Schlegel HB, Scuseria GE, Robb MA, Cheeseman JR, Zakrzewski VG, Montgomery JA, Stratmann JCBRE, Dapprich S, Millam JM, Daniels AD, Kudin KN, Strain MC, Farkas O, Tomasi J, Barone V, Cossi M, Cammi R, Mennucci B, Pomelli C, Adamo C, Clifford S, Ochterski J, Petersson GA, Ayala PY, Cui Q, Morokuma K, Malick DK, Rabuck AD, Raghavachari K, Foresman JB, Cioslowski J, Ortiz JV, Baboul AG, Stefanov BB, Liu ALG, Piskorz IKP, Gomperts R, Martin RL, Fox DJ, Keith T, Al-Laham MA, Peng CY, Nanayakkara A, Gonzalez C, Challacombe M, Gill PMW, Johnson BG, Chen W, Wong MW, Andres JL, Head-Gordon M, Replogle ES, Pople JA (2003) GAUSSIAN 03 (revision A.9). Gaussian Inc, Pittsburgh
51. Ohno K, Komuro M, Sugaya T, Nagasawa A, Fujihara T (2020) Dalton Trans 49:1873–1882
52. Erkan S, Karakaş D (2019) Chem Pap 73:2387–2398
53. Li J, Han D, Gao J, Chen T, Wang B, Shang X (2020) RSC Adv 10:18519–18525
54. Tamukong PK, Peiris WD, Kilina S (2016) PCCP 18:20499–20510
55. Frisch A, Nielson AB, Holder AJ (2000) Gaussian Inc. Pittsburgh, PA
56. Jimenez J, Pinto MN, Martinez-Gonzalez J, Mascharak PK (2019) Inorg Chim Acta 485:112–117